Electrical properties of iron-silica nanocomposites synthesized by electrodeposition

S. Banerjee, A. K. Ghosh, and D. Chakravorty

Citation: Journal of Applied Physics **86**, 6835 (1999); doi: 10.1063/1.371759
View online: http://dx.doi.org/10.1063/1.371759
View Table of Contents: http://scitation.aip.org/content/aip/journal/jap/86/12?ver=pdfcov
Published by the AIP Publishing

Electrical properties of iron-silica nanocomposites synthesized by electrodeposition

S. Banerjee, A. K. Ghosh, and D. Chakravorty[a)]
Indian Association for the Cultivation of Science, Jadavpur, Calcutta 700 032, India

(Received 2 June 1999; accepted for publication 11 August 1999)

Nanometer-sized iron particles with diameters in the range 5.5–11.1 nm were grown within a silica gel by an electrodeposition method. Electron diffraction measurements show that some of the iron particles were oxidized to Fe_3O_4. dc resistivity measurements over the temperature range 110–300 K show a $T^{-1/4}$ variation indicating a variable range hopping transport. ac conductivity over the frequency range 100 Hz–2 MHz show an overlapping large polaron tunneling mechanism to be operative. The dielectric modulus spectra as a function of frequency were analyzed on the basis of a stretched exponential relaxation function. The values of the exponent β as extracted from this analysis were in the range 0.38–0.46. The activation energies corresponding to the maximum of the imaginary part of the dielectric modulus were in the range 0.13–0.20 eV. These are ascribed to an electron tunneling mechanism. © *1999 American Institute of Physics.* [S0021-8979(99)01522-4]

I. INTRODUCTION

Nanocomposites have attracted considerable attention in recent years because of useful and unusual properties exhibited by them.[1–3] Several physical and chemical methods have been reported for the preparation of such materials.[4–12] An electrodeposition method has been found to be effective in synthesizing nanocomposites involving a metallic phase.[12] We have used this method to grow nanometer-sized iron particles within a silica gel matrix. Electrical conduction shows an interesting behavior. We report on the details in this article.

II. EXPERIMENT

Two gels with target compositions $10\,FeCl_3 \cdot 90\,SiO_2$ (mol %) and $15\,FeCl_3 \cdot 85\,SiO_2$ (mol %), respectively, were prepared. The starting materials used were anhydrous $FeCl_3$, tetraethylorthosilicate, ethyl alcohol, and distilled water. A measured amount of $FeCl_3$ was dissolved in distilled water and ethyl alcohol and the solution was stirred in a magnetic stirrer. Tetraethylorthosilicate with half the volume of distilled water and ethyl alcohol was added to the latter solution and one drop of concentrated HCl was added. The *p*H of the resulting solution was found to be ~5. Stirring of this solution was continued for 3 h. A transparent sol was obtained. The latter was kept in a flat bottomed petri dish in ordinary atmosphere for two weeks for gelation. Gel pieces of size ~5 mm×5 mm×1 mm were obtained after this process. These were crushed in a mortar to an approximate size of 5 μm. The powder had a faint yellow color.

For electrodeposition a polished iron cathode of dimension 2.5 cm×2.5 cm×1 mm and iron anode having dimension 3 cm×1 cm×1 mm were used. A thick gel paste was prepared by mixing 10 mg of the gel powder synthesized as described above with 0.2 c.c. of distilled water. The cathode surface was coated with this paste. After placing the anode on the surface of the gel paste the electrodeposition was carried out at two different voltages viz., 10 and 20 V, respectively. The voltage was kept on for a typical duration of 20 s. The deposition current increased from a few microamperes to ~1 A indicating the formation of metallic channels within the gel. By changing the position of the anode formation of metal phase was brought about within the entire gel mass. On completion of the electrodeposition the gel mass turned black. The gel was dried in a flow of hot air at 333 K for a few minutes. The gel powder was then scraped off the cathode surface. The powder thus collected was kept in a vacuum chamber at 373 K for 30 h. Taking this powder in a mold and applying a pressure of 3 tons/cm^2 for 30 min pellets of area ~0.7 cm^2 and thickness ~1 mm were prepared.

The microstructure of these powders were studied by a JEM 200 CX transmission electron microscope. Details of specimen preparation have been described elsewhere.[13]

Electrical measurements were carried out on pellet specimens coated on opposite faces by silver paint supplied by Acheson Colloiden BV Holland. dc resistance of the specimens was measured over the temperature range 110–300 K by a Keithley 617 electrometer. The ac impedance was measured over the frequency range 100 Hz–2 MHz using a Hewlett Packard HP 4192A impedance analyzer.

III. RESULTS AND DISCUSSION

Figure 1(a) shows the transmission electron micrograph of the specimen with composition $15\,FeCl_3$, $85\,SiO_2$, and subjected to an electrodeposition voltage of 20 V. Figure 1(b) is the electron diffraction pattern obtained from Fig. 1(a). The diffraction rings indicate the presence of crystalline phase (s) in the specimen. The interplanar spacing d_{hkl} values were calculated from diameters of these rings and the results are listed in Table I. It is evident from this table that the particles seen in Fig. 1(a) are comprised of the α iron.

a)Also affiliated with Jawaharlal Nehru Center for Advanced Scientific Research, Bangalore 560 064, India, electronic mail: mlsdc@mahendra.iacs.res.in

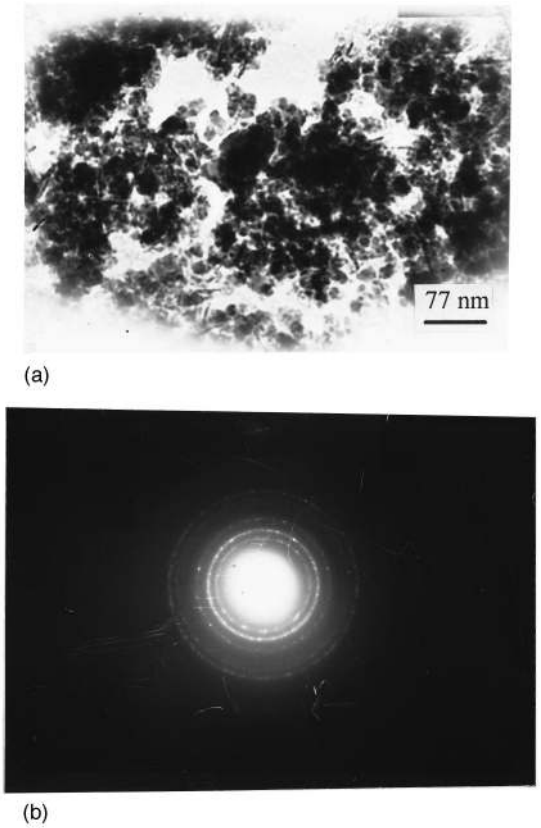

FIG. 1. (a) Transmission electron micrograph for specimen No. 1; (b) electron diffraction pattern obtained from (a).

Some lines corresponding to Fe_3O_4 indicate that some of the iron particles have been partially oxidized. These results are typical of all the three samples studied. Shown in Fig. 2 is the histogram of iron particles as obtained from Fig. 1(a). The line in this figure is the theoretical curve drawn by least-squares fitting of the experimental data to a log-normal distribution function.[14] In Table II we have summarized the values of median diameter $\bar{x}$ and geometric standard deviation σ as extracted by the above fitting to the histograms of different specimens. It is evident from this table that the median diameters of iron particles in the present series of specimens have values in the range 5.5–11.1 nm. The diameters depend on the concentration of iron ions in the precursor gel as well as the voltage used for electrodeposition—the particle size decreasing with an increase in iron concentration or an increase in the applied voltage. This has been previously explained as arising due to the dielectric breakdown model (DBM) being operative in this system.[15,16] The model was used in the case of growth of copper in a liquid electrolyte[15] and silver in a gel medium.[16] The same explanation holds in the present specimens because experimental conditions are similar in all the cases.

TABLE I. Comparison of interplanar spacings d_{hkl} obtained for specimen 15 $FeCl_3$ ·85 SiO_2 subjected to 20 V electrodeposition treatment with standard ASTM data.

	ASTM	
Observed (nm)	α-Fe (nm)	Fe_3O_4 (nm)
0.203	0.20266	
0.174		0.1712
0.144	0.14332	
0.118	0.11702	
0.110		0.1092
0.101	0.10134	
0.091	0.09064	

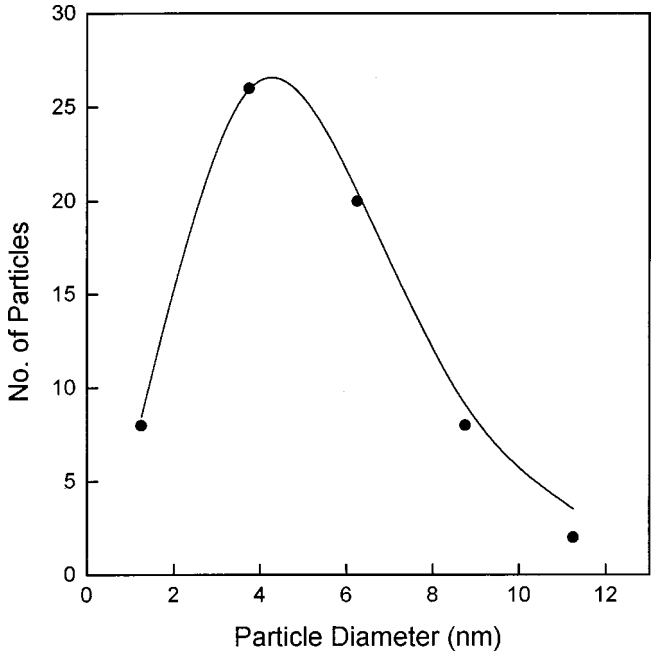

FIG. 2. Histogram of particle size obtained from Fig. 1(a).

Figure 3 shows the variation of logarithm of resistivity as a function of $T^{-1/4}$ for different specimens (T being the temperature). It is evident all the specimens exhibit a linear variation. In this figure the points represent the experimental data and the solid lines are the theoretically fitted curves to the equation governing the variable range hopping model viz.,

$$\rho = \rho_0 \exp\left(\frac{T_0}{T}\right)^{1/4}, \tag{1}$$

where, ρ is the resistivity, ρ_0 the preexponential factor and

$$T_0 = \frac{8 b_c \chi^3}{f N(E_F) k}. \tag{2}$$

In the above equation b_c is a dimensionless number having a value 1.5,[17] χ is the tunneling constant,[18] f is a proportional-

TABLE II. Summary of median diameter $\bar{x}$ and geometric standard deviation σ for different specimens.

Specimen No.	Composition	Electrodeposition voltage (V)	Median diameter $\bar{x}$ (nm)	Geometric standard deviation σ
1	15 $FeCl_3$ 85 SiO_2	20	5.5	1.6
2	10 $FeCl_3$ 90 SiO_2	20	9.5	1.4
3	10 $FeCl_3$ 90 SiO_2	10	11.1	1.6

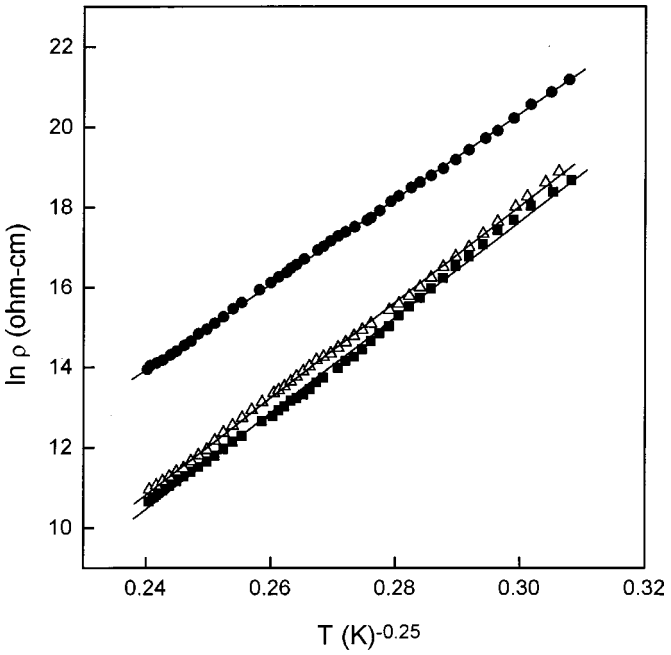

FIG. 3. Variation of logarithm resistivity as a function of $T^{-1/4}$; specimen 1 (●); specimen 2 (△); specimen 3 (■).

ity constant, $N(E_F)$ is the density of states in the vicinity of the Fermi level, and k is the Boltzmann constant. It is evident that in the present specimen system the electrical resistivity is controlled by a variable range hopping mechanism over the entire temperature range of measurement, viz., 110–300 K. Usually a composite of nanosized metal particles and an oxide phase exhibit a $T^{1/2}$ variation in this temperature range.[19] This has been shown to arise due to an electron tunneling mechanism between neighboring metallic islands. In the present system there being a distribution of metal particle diameter in the range 2–16 nm the activation energy for tunneling should also vary over a wide range. The expression for activation energy ϕ is given by[20]

$$\phi = \frac{1.44}{\epsilon}\left(\frac{2}{r} - \frac{1}{(r/2)+p}\right)\text{eV}, \tag{3}$$

where, r is the particle diameter, p is the separation between the particles both expressed in nanometers, and ϵ is the dielectric constant of the gel medium. Using the values of $p = 2$ nm and the median diameter $\bar{x}$ for different specimens we obtain activation energy values of 0.18 eV (for $r = 2$ nm) and 0.06, 0.04, and 0.03 eV, respectively. In this calculation we have taken $p-r$ which is a reasonable assumption. The total resistivity of any specimen can therefore be written as

$$\rho = \sum_i \omega_i \rho_{0i} e^{\phi_i/kT}, \tag{4}$$

where, i represents the effective resistance elements arising due to different activation energies ϕ_i, k the Boltzmann constant, ρ_{0i} the preexponential factor, ω_i the weight factor, and T the temperature. We can write to a first approximation from Eq. (4):

$$\rho = \rho_{01}\exp(\phi_1/kT) + \omega_2\rho_{02}\exp(\phi_2/kT), \tag{5}$$

TABLE III. $N(E_F)$ values for different specimens calculated from dc resistivity data.

Specimen No.	$N(E_F)$ (eV^{-1} c.c.$^{-1}$)
1	6.8×10^{18}
2	6.7×10^{18}
3	1.1×10^{19}

where ϕ_1 refers to the activation energy due to the median diameter and ϕ_2 that due to particles with diameter ~2 nm. Typical values for ω_1 and ω_2 are 0.78 and 0.22, respectively. Taking $\rho_{01} \simeq \rho_{02}$ because the preexponential factor is more or less constant for a particular volume fraction of metal,[18] it can be seen from Eq. (5) that the temperature variation of resistivity will be controlled by the second term. Thus a variable range hopping mechanism will be preferable for the localized carriers.[19] It should be mentioned here that the nanocomposites of the present series can be described as a disordered system with a density of states function near the Fermi level[21] denoted by $N(E_F)$ as shown in Eq. (2). Taking $f=1$, $b_c=1.5$ and calculating the value of the tunneling constant χ ($\sim 0.22\,\text{A}^{0-1}$) from the equation

$$\chi = \sqrt{\frac{2m\phi}{h^2}}, \tag{6}$$

where, m is the electron mass, ϕ the barrier height (=ionization potential-electron affinity) the values of $N(E_F)$ were calculated for different specimens. These are summarized in Table III. It is evident that the density of states is of the order of $10^{19}\,\text{eV}^{-1}$ c.c.$^{-1}$. Multiplying it with kT_r where T_r is the room temperature (300 K) we obtain values of the total number of states for the three specimens as 1.7×10^{17}, 1.7×10^{17}, and 2.7×10^{17}/c.c., respectively. From the electron micrographs of the specimens it is found that the number of iron particles is $\sim 5\times10^{17}$/c.c. This is of the same order of magnitude as the total number of states estimated above. It is therefore concluded that the variable range hopping conduction mechanism controlling the dc resistivity variation as a function of temperature occurs due to the localized density of states near the Fermi level of a disordered medium formed by the iron nanoparticles.

Figure 4 shows the variation of ac conductivity as a function of frequency at different temperatures for specimen No. 1. The points represent the experimental data. This is typical of other specimens. These data were fitted to the following equation viz.,

$$\sigma_t = \sigma_{\text{dc}} + A\omega^s, \tag{7}$$

where, σ_t is the measured ac conductivity, σ_{dc} the dc part of the conductivity, A a constant, ω the angular frequency, and s the frequency exponent. Shown in Fig. 5 is the variation of s obtained by the above procedure as a function temperature in the case of specimen No. 1.

A number of theories have been proposed to explain the ac conductivity behavior in amorphous materials using the concept of localized states.[22,23] The nature of variation of s in our specimens indicate that the overlapping large polaron

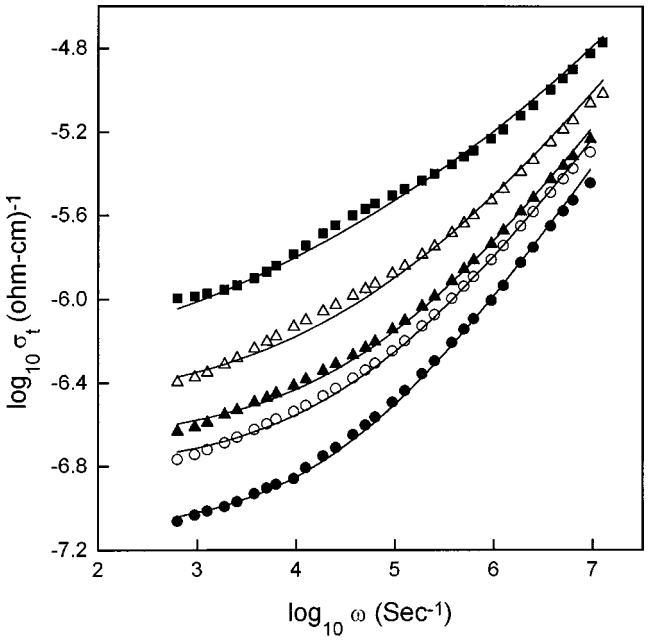

FIG. 4. Variation of ac conductivity as a function of frequency for specimen No. 1 at different temperatures; (■) 306.5 K, (△) 266.8 K, (▲) 244.7 K, (○) 238.5 K, and (●) 217.3 K.

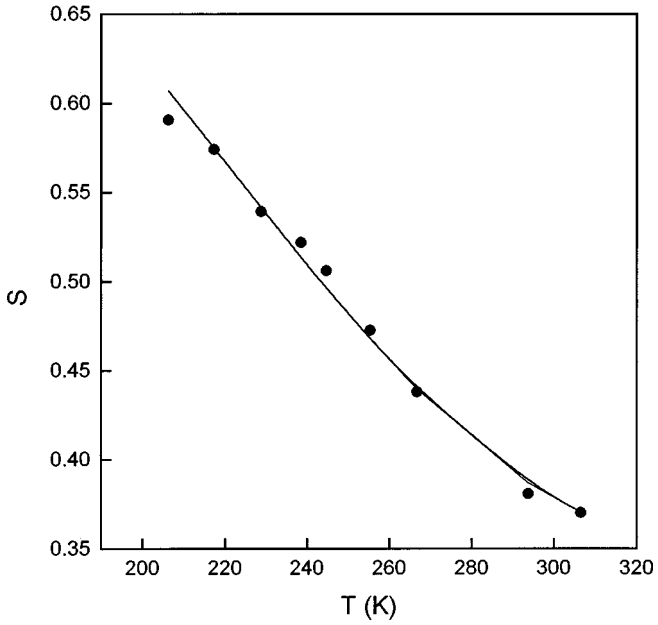

FIG. 5. Variation of s as a function of temperature for specimen No. 1.

tunneling (OLPT) mechanism is operative here. According to this model[22] the polaron hopping energy W_H is given by

$$W_H = W_{HO}(1 - r_p/R_W), \tag{8}$$

where r_p is the polaron radius and R_W is the tunneling distance. R_W can be written as

$$R_W = \frac{1}{4\alpha}\left[\ln\left(\frac{1}{\omega\tau_0}\right) - \frac{W_{HO}}{kT}\right] + \frac{1}{4\alpha}\left\{\left[\ln\left(\frac{1}{\omega\tau_0}\right) - \frac{W_{HO}}{kT}\right]^2 + \frac{8\alpha r_p W_{HO}}{T}\right\}^{1/2}. \tag{9}$$

In this equation α is the spatial extent of the polaron, τ_0 is the characteristic relaxation time and is of the order of the inverse phonon frequency, k the Boltzmann constant, and T the temperature.

The expressions for ac conductivity $\sigma(\omega)$ and frequency exponent s are as follows:

$$\sigma(\omega) = \frac{\pi^4}{12} e^2 (kT)^2 [N'(E_F)]^2 \frac{\omega R_W^4}{2\alpha kT + W_{HO} r_p / R_W^2}, \tag{10}$$

$$s = 1 - \frac{8\alpha R_W + 6 W_{HO} r_p / R_W kT}{(2\alpha R_W + W_{HO} r_p / R_W kT)^2}, \tag{11}$$

where e is the electronic charge and $N'(E_F)$ is the density of states at the Fermi level.

The ac conductivity data for the specimens were fitted to Eqs. (9), (10), and (11) using α, W_H, r_p, τ_0, and $N'(E_F)$ as parameters. The solid lines in Fig. 4 are the theoretically fitted curves. Table IV summarizes the values of the parameters obtained at different temperatures. These values have been calculated for a frequency 10 kHz. In order to get an insight into the physical mechanism responsible for the polaron tunneling we obtain the total number of states at room temperature by multiplying $N'(E_F)$ with kT_r where T_r is 300 K. This is found to have a value $\sim 2.5\times 10^{21}$/c.c. for specimen No. 3 and $\sim 3.4\times 10^{21}$/c.c. for specimen No.1.

TABLE IV. Values of α, W_H, r_p, τ_0, and $N'(E_F)$ as extracted by least-square fitting of $\sigma(\omega)$ to OLPT model.

Specimen No.	Temperature (K)	α (A^{0-1})	W_H (eV)	r_p (A^0)	τ_0 (s)	$N'(E_F)$ (eV^{-1} c.c.$^{-1}$)
1	306.5	0.34	0.48	1.2	5.0×10^{-13}	1.4×10^{23}
	267	⋯	⋯	⋯	⋯	1.5×10^{23}
	245	⋯	⋯	⋯	⋯	1.7×10^{23}
	238.0	⋯	⋯	⋯	⋯	1.7×10^{23}
	217.0	⋯	⋯	⋯	⋯	1.9×10^{23}
2	298.5	0.36	0.46	1.3	5.0×10^{-13}	1.0×10^{23}
	280	⋯	⋯	⋯	⋯	1.1×10^{23}
	261	⋯	⋯	⋯	⋯	1.2×10^{23}
	240	⋯	⋯	⋯	⋯	1.2×10^{23}
	209	⋯	⋯	⋯	⋯	1.4×10^{23}

From the chemical compositions of the gels used we have calculated the iron ion concentrations for these specimens as 2.6×10^{21} and as 3.6×10^{21}/c.c., respectively. It is evident therefore that the iron ions form the polaronic sites in these cases. For the hopping to take place iron ions must exist in two valence states, e.g., Fe^{2+} and Fe^{3+}. We have tried to confirm the presence of Fe^{2+} ions in the original gel powder (before the electrodeposition step) by dissolving the latter in a solution made of 1:1 H_2SO_4 and HF, respectively, in nitrogen atmosphere. Orthophenanthroline was dissolved in ethyl alcohol and added to the solution. This did not produce any blood red coloration thereby indicating the absence of Fe^{2+} ions.[24] We have already reported earlier in this article that Fe_3O_4 phase forms on the nanosized iron particles. Variable valence iron ion sites are thus provided by Fe_3O_4 phase and the gel matrix, respectively. It should be pointed out that Fe_3O_4 contains both Fe^{2+} and Fe^{3+} ions.[25]

Last, we have investigated the dielectric modulus spectra of the present series of samples and analyzed the data in terms of stretched exponential relaxation.[26]

The dielectric modulus M^* is defined as

$$M^* = M_1 + jM_2 = \frac{1}{\epsilon^*}, \tag{12}$$

where ϵ^* the complex dielectric permittivity is given by

$$\epsilon^* = \epsilon_1 + j\epsilon_2 . \tag{13}$$

We write the Kohlrausch–Williams–Watts (KWW) stretched exponential relaxation function $F(t)$ as[27]

$$F(t) = \exp(-t/\tau_R)^{\beta}, \tag{14}$$

where τ_R is the conductivity relaxation tune and β the exponent. It can be shown that the real and imaginary parts of M^* are given by

$$M_1(\omega) = M_s\left(1 - \sum_{i=1}^{m} \frac{g_i}{1+(\omega\lambda_i\tau_R)^2}\right) \tag{15}$$

$$M_2(\omega) = M_s \sum_{i=1}^{m} \frac{\omega g_i \lambda_t \tau_R}{1+(\omega\lambda_i\tau_R)^2}, \tag{16}$$

where

$$M_s = \frac{1}{\epsilon_a} \tag{17}$$

and

$$\lambda_i = \tau_i/\tau_R , \tag{18}$$

τ_i being multiples of τ_R and are selected to cover a suitable range of (t/τ_R) in which $F(t)$ has an appreciable time dependence. Equations (15) and (16) were fitted to the experimental dielectric modulus data by a least-square method. The details have been reported earlier.[28] Figure 6 shows the normalized plots of both real and imaginary parts of dielectric modulus as a function of frequency for specimen No. 3 at different temperatures. It should be noted that ω_0 is the angular frequency at which M_2 has the maximum value. The points in this figure represent the experimental data and the lines are the theoretical fits to Eqs. (15) and (16). The agreement between the two is remarkable. This is typical of the dielectric modulus data for the other specimens.

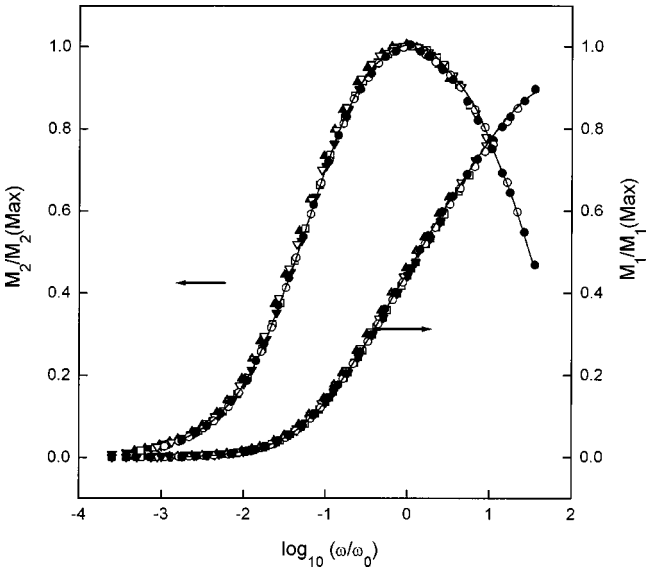

FIG. 6. Real and imaginary parts of dielectric modulus as a function of frequency for specimen No. 3; (▼) 251.0 K, (▲) 239.7 K, (□) 225.9 K, (▽) 209.4 K, (○) 186.6 K, (●) 173.6 K.

The β values for the different specimens were extracted by the procedure described earlier.[28] These are summarized in Table V. It is evident that as the particle size is reduced the value of β also tends to decrease. This implies that the distribution of relaxation times becomes wider as the particle size becomes smaller. It is also interesting to note that the curves and data for different temperatures in the normalized plots overlap perfectly over the entire frequency spectrum. This is indicative of the fact that the value of β does not change with temperature. This means the distribution function for relaxation times in the case of all the specimens does not change with temperature.

In Fig. 7 the logarithm of ω_0 is plotted as a function of inverse temperature for specimen No. 3. Evidently the data fall on a straight line. From the slope of this line we have calculated the activation energy for the mechanism concerned. The activation energy values for different specimens are listed in the last column of Table V. The values are seen to vary between 0.20 and 0.13 eV as the particle size is increased from 5.5 to 11.1 nm. From a previous discussion we recall that an electron tunneling mechanism between metallic islands will cause an activation energy ~0.2 eV if the particle diameter is ~2 nm. From the histogram of specimen No. 1 (Fig. 2) it is evident that a sizable fraction of particles have diameters ~2 nm. We have estimated from Eq. (3) that

TABLE V. Summary of the values of stretched exponential parameter β and activation energy for dielectric dispersion for different specimens.

Specimen No.	β	Activation energy (eV)
1	0.38±0.006	0.20
2	0.48±0.005	0.14
3	0.46±0.003	0.13

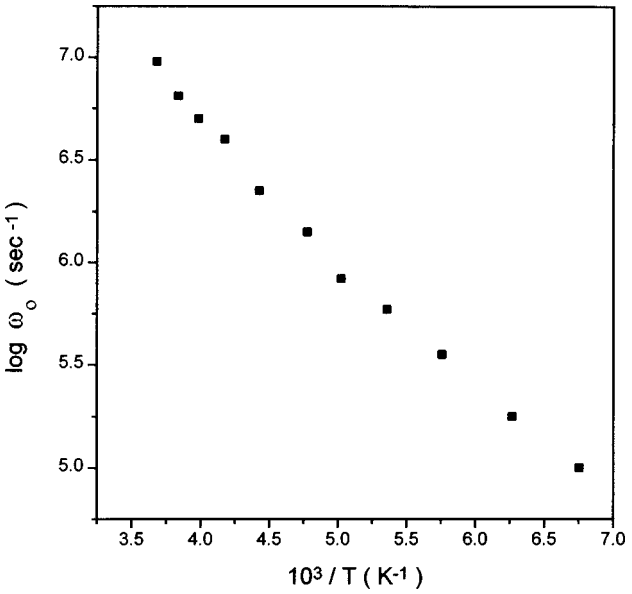

FIG. 7. The logarithm of ω_0 is plotted as a function of inverse temperature for specimen No. 3.

the values of r are necessary to obtain the activation energy values of 0.14 and 0.13 eV for specimens 2 and 3, respectively. These are found to be 3.4 and 3.7 nm, respectively. The histograms of these specimens also show a distribution covering these sizes.

In summary, we have synthesized iron-silica gel nanocomposites by an electrodeposition method. The metal particle sizes vary from 5.5 to 11.1 nm depending on the gel composition and the voltage applied. The dc resistivity over the temperature range 110–300 K shows a variable range hopping transport. The ac conductivity measured over the frequency range 100 Hz–2 MHz indicates that an OLPT mechanism is operative. The Fe^{2+} and Fe^{3+} sites are provided by the Fe_3O_4 phase and the gel matrix. The dielectric modulus dispersion study shows values of KWW exponent β in the range 0.38–0.46. This arises due to the electron tunneling mechanism between the metal particles.

ACKNOWLEDGMENT

This research has been supported by the Department of Science and Technology, Government of India, New Delhi.

[1] A. I. Ekimov and A. A. Onushchenko, Zh. Eksp. Teor. Fiz. **40**, 337 (1984); [JETP Lett. **40**, 1136 (1984)].
[2] Y. Wang, N. Herron, W. Mahler, and A. Suna, J. Opt. Soc. Am. B **6**, 808 (1998).
[3] B. O. Dabbonsi, M. Bawendi, O. Onitsuka, and M. F. Rubner, Appl. Phys. Lett. **66**, 1316 (1995).
[4] G. Riegel and J. R. Bolton, J. Phys. Chem. **99**, 4215 (1995).
[5] A. P. Alivisatos, Science **271**, 933 (1996).
[6] K. Rajeshwar, Adv. Mater. **4**, 23 (1992).
[7] B. E. Breyfogel, M. G. Shumsky, C-J. Hung, and J. A. Switzer, J. Electrochem. Soc. **143**, 2741 (1996).
[8] C. Martin, Science **266**, 1961 (1994).
[9] H. Hahn and R. S. Averback, J. Appl. Phys. **67**, 1113 (1990).
[10] M. Shiratani, T. Fukuzawa, and T. Watanabe, IEEE Trans. Plasma Sci. **22**, 103 (1994).
[11] T. K. Kundu and D. Chakravorty, Appl. Phys. Lett. **67**, 2732 (1995).
[12] S. Banerjee and D. Chakravorty, Appl. Phys. Lett. **72**, 1027 (1998).
[13] A. K. Maity, D. Nath, and D. Chakravorty, J. Phys.: Condens. Matter **8**, 5717 (1996).
[14] B. Roy and D. Chakravorty, J. Phys.: Condens. Matter **2**, 9323 (1990).
[15] V. Fleury, Nature (London) **390**, 145 (1997).
[16] S. Banerjee, S. Banerjee, A. Datta, and D. Chakravorty, Europhys. Lett. **46**, 346 (1999).
[17] P. Sheng and J. Klafter, Phys. Rev. B **27**, 1583 (1993).
[18] B. Abeles, P. Sheng, M. D. Coutts, and Y. Arie, Adv. Phys. **24**, 407 (1975).
[19] P. Sheng, in *Nanophase Materials*, edited by G. C. Hadjipanayis and R. W. Siegel (Kluwer, The Netherlands, 1994), p. 381.
[20] P. A. Tick and F. P. Fehlner, J. Appl. Phys. **43**, 362 (1962).
[21] S. Banerjee and D. Chakravorty, J. Appl. Phys. **84**, 1149 (1998).
[22] A. R. Long, Adv. Phys. **31**, 553 (1982).
[23] N. F. Mott and E. A. Davis, *Electronic Processes in Non-Crystalline Materials*, 2nd ed. (Oxford, Clarendon, 1979), p. 225.
[24] D. Nicholls, *The Chemistry of Iron, Cobalt and Nickel* (Pergamon International Library, Oxford and New York, 1973), p. 1027.
[25] W. D. Kingery, *Introduction to Ceramics* (Wiley, New York, 1967), p. 680.
[26] P. K. Dixon, L. Wu, S. R. Nagel, B. D. Williams, and J. P. Cariai, Phys. Rev. Lett. **65**, 1108 (1990).
[27] P. B. Macedo, C. T. Moynihan, and R. Bose, Phys. Chem. Glasses **13**, 171 (1972).
[28] S. K. Saha and D. Chakravorty, J. Phys. D **23**, 1201 (1990).